Hidden Plaquette Order in a Classical Spin Liquid Stabilized by Strong Off-Diagonal Exchange

Preetha Saha, Zhijie Fan, Depei Zhang, and Gia-Wei Chern

Phys. Rev. Lett. **122**, 257204 — Published 28 June 2019

DOI: 10.1103/PhysRevLett.122.257204

Hidden plaquette order in classical spin liquid stabilized by strong off-diagonal exchange

Preetha Saha, Zhijie Fan, Depei Zhang, and Gia-Wei Chern
Department of Physics, University of Virginia, Charlottesville, VA 22904, USA
(Dated: June 10, 2019)

We report a new classical spin liquid in which the collective flux degrees of freedom break the translation symmetry of the honeycomb lattice. This exotic phase exists in the frustrated spin-orbit magnets where a dominant off-diagonal exchange, the so-called Γ term, results in a macroscopic ground-state degeneracy at the classical level. We demonstrate that the system undergoes a phase transition driven by thermal order-by-disorder at a critical temperature $T_c \approx 0.04|\Gamma|$. This transition reduces the emergent spherical spin-symmetry to a cubic one: spins point predominantly toward the cubic axes, yet seem to remain disordered at $T < T_c$. Importantly, we show that the phase transition corresponds to a hidden plaquette ordering of hexagonal fluxes which explicitly breaks the cubic symmetry, a scenario that is confirmed by our extensive Monte Carlo simulations. We further compute the dynamical structure factors of the spin-liquid phase and reveal unusual dynamical properties of the hexagonal flux parameters.

Mott insulators with strong spin-orbit coupling have generated considerable interest recently [1]. The local magnetic degrees of freedom in such materials are entities with significant orbital character. This special property leads to effective interactions that exhibit strong anisotropy in both real and pseudo-spin spaces, as described by Hamiltonians such as quantum compass or 120° models [2, 3]. A new type of magnetic frustration [4–6], which is different from the well studied geometrical frustration [7–10], originates from the nontrivial interplay between lattice geometry and anisotropic spin-orbital exchange. One recent representative example is the spin-1/2 honeycomb Kitaev model [11] with Ising-like interactions involving different spin components on the three distinct nearest-neighbor bonds. Remarkably, the Kitaev model is exactly solvable and exhibits a quantum spin-liquid ground state with fractionalized excitations [11–13]. The classical limit of the Kitaev Hamiltonian also exhibits a macroscopic ground-state degeneracy and interesting order-by-disorder phenomena [14–17].

The recent enormous interest in frustrated spin-orbit magnets is triggered by the realization that spin interactions in certain $4d$ and $5d$ Mott insulators are dominated by the anisotropic Kitaev-type exchange [18–21]. The presence of other spin interactions, notably the isotropic Heisenberg exchange, in these compounds eventually drives the system into a magnetically ordered state despite a dominate Kitaev term [22–33]. Nevertheless, the search for spin liquids in frustrated spin-orbit magnets continues. Experimentally, tuning spin interactions by applying magnetic field [34–36] or pressure [37, 38] has been attempted to suppress the magnetic order. On the theoretical side, it has been pointed out that the off-diagonal exchange anisotropy, the so-called Γ term, plays a crucial role in the magnetic behaviors of these spin-orbit Mott insulators [39–45]. In fact, the suppression of long-range order in some compounds is suspected to be due to the increased strength of Γ interaction, instead of the enhanced Kitaev-type exchange [46–49]. This experimental tendency can be understood from a recent theoretical work that shows a new classical spin liquid in the idealized Γ model on the honeycomb lattice and its three-dimensional variants [50].

In this paper, we investigate the thermodynamic behavior of the Γ model at low temperatures and demonstrate a phase transition driven by order-by-disorder at $T_c \approx 0.04\,|\Gamma|$. Importantly, we show a hidden plaquette order that breaks the lattice transition symmetry below T_c. To begin with, we consider the Γ model on the honeycomb lattice, in which nearest-neighbor (NN) spin interaction is dominated by the off-diagonal exchange term. It involves different spin-components on the three inequivalent NN bonds, denoted as x, y, and z (see Fig. 1), on the honeycomb lattice:

$$\mathcal{H} = \Gamma \sum_{\gamma} \sum_{\langle ij \rangle \| \gamma} (S_i^{\alpha} S_j^{\beta} + S_i^{\beta} S_j^{\alpha}). \tag{1}$$

Here (α, β, γ) are permutations of (x, y, z). The classical ground states of Γ model are extensively degenerate [50], giving rise to a new type of classical spin liquid that is different from the familiar cases in geometrical frustrated magnets. Our Monte Carlo (MC) simulations show no sign of phase transition down to $T \sim 0.05|\Gamma|$ [51]. The energy density gradually approaches its minimum $E_0 = -|\Gamma|$, while the specific heat shows a plateau-like feature at $T \lesssim 0.1\,|\Gamma|$. The static structure factor for $\Gamma > 0$ exhibits a broad minima at $\mathbf{q} = 0$ at $T = 0.05|\Gamma|$ [51]. MC simulations further find extremely short-ranged spin-spin correlation, which is similar to that seen in Kitaev spin liquid [11, 14], but different from that of geometrical frustrated systems [52–54].

The characterization of the degenerate ground-state manifold has been discussed in great detail in Ref. [50]. A generic ground state is specified by a directional vector $\hat{\mathbf{n}} = (a, b, c)$ and a set of Ising variables $\{\eta_\alpha\}$ defined on individual hexagons; see Fig. 1. In the classical limit,

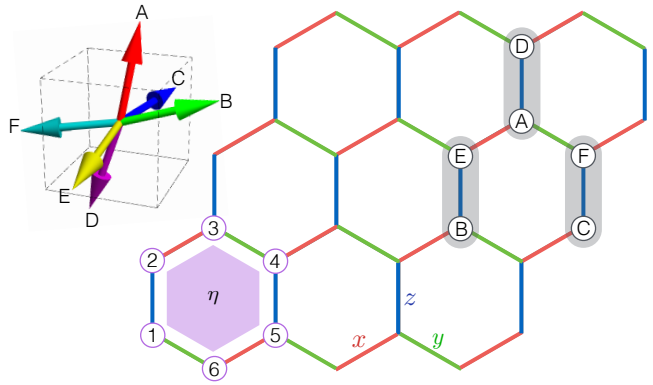

FIG. 1. (Color online) Ground states of the Γ model on a honeycomb lattice. A generic ground state is characterized by a directional vector $\hat{\mathbf{n}} = (a, b, c)$ and a set of Ising variables $\{\eta_\alpha\}$ defined on individual hexagons. To construct a ground state, first we build a perfect $\sqrt{3} \times \sqrt{3}$ order based on the six inequivalent spins of the tripled unit cell: $\mathbf{S}_{\rm A} = (a, b, c)$, $\mathbf{S}_{\rm B} = (c, a, b)$, $\mathbf{S}_{\rm C} = (b, c, a)$, $\mathbf{S}_{\rm D} = \zeta(b, a, c)$, $\mathbf{S}_{\rm E} = \zeta(a, c, b)$, and $\mathbf{S}_{\rm F} = \zeta(c, b, a)$. Here $\zeta = -\mathrm{sgn}(\Gamma)$. Next, go through every hexagon and modify the component of its six spins: $S_1^x \to \eta S_1^x$, $S_2^y \to \eta S_2^y$, $S_3^z \to \eta S_3^z$, $S_4^x \to \eta S_4^x$, $S_5^y \to \eta S_5^y$, and $S_6^z \to \eta S_6^z$. In the example shown above, $\zeta = -1$. The spins of shaded hexagon at the lower left corner are: $\mathbf{S}_1 = (a, b, c)$, $\mathbf{S}_2 = \zeta(b, a, c)$, $\mathbf{S}_3 = (b, c, a)$, $\mathbf{S}_4 = \zeta(a, c, b)$, $\mathbf{S}_5 = (c, a, b)$, and $\mathbf{S}_6 = \zeta(c, b, a)$.

these Ising variables are pure gauge degrees of freedom and will remain disordered at all temperatures. An explicit procedure for constructing the ground state characterized by $\hat{\mathbf{n}}$ and $\{\eta_\alpha\}$ starting from the perfect $\sqrt{3} \times \sqrt{3}$ spin order is detailed in Fig. 1. Note that the eight directions $(\pm a, \pm b, \pm c)$ correspond to the same $\hat{\mathbf{n}}$ as they are related by flipping the η variable. It is thus similar to the director in nematic liquid crystal.

One important question regarding the dynamics of the ground state is whether the different Ising sectors $\{\eta_\alpha\}$ are fully connected. It turns out continuous transformation of $\{\eta_\alpha\}$ can be achieved with the aid of the directional vector $\hat{\mathbf{n}} = (a, b, c)$. To see this, we first note that each η_α is associated with only *one* component of the unit vector $\hat{\mathbf{n}}$ in the ground state. Take the hexagon shown in Fig. 1 as an example. According to the ground-state rule, the local η only controls the 'a'-component of the six spins in this hexagon. As a result, all η-variables can be divided into three groups: type-A (respectively, B and C) for spin-components controlled by a (respectively, b and c). When one of the component of $\hat{\mathbf{n}}$ vanishes, 1/3 of the η becomes idle. This feature allows us to construct a continuous path from one set of η to another one η' by rotating $\hat{\mathbf{n}}$ according to the sequence: $(a, b, c) \to (0, b', c') \to (a'', 0, c'') \to (a''', b''', 0) \to (a, b, c)$. After the first rotation, the vanishing a component allows us to change 1/3 of the η variables (those associated with a-component) to their counterpart in η'. Repeating similar process for the other two sets of η then completes the transformation from η to η' while keeping the $\hat{\mathbf{n}}$ vector in the same direction.

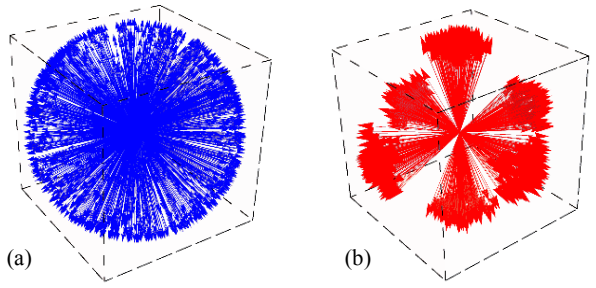

FIG. 2. (Color online) Snapshots of spin configurations above and below $T_c = 0.0401|\Gamma|$: (a) $T = 0.05$ and (b) $T = 0.03$. In the low-T phase, spins predominately point toward the six cubic directions.

The above discussion also shows that without the rotational symmetry of $\hat{\mathbf{n}}$, different $\{\eta_\alpha\}$ becomes disjoint from each other. Interestingly, our MC simulations find a freezing phenomenon of the vector $\hat{\mathbf{n}}$ at a very low temperature $T_c \approx 0.04\,|\Gamma|$, as demonstrated in Fig. 2. At $T > T_c$, the spins and $\hat{\mathbf{n}}$ exhibit an emergent spherical symmetry even at temperatures well below the exchange energy scale $|\Gamma|$. This rotational symmetry is lost below T_c, and spins mainly point toward the six cubic axes, or equivalently the directional vector freezes to one of the cubic directions, i.e. $\hat{\mathbf{n}} \sim (1, 0, 0)$, $(0, 1, 0)$, or $(0, 0, 1)$. As states parameterized by different $\hat{\mathbf{n}}$ are degenerate at the mean-field level, the cubic directions are selected by thermal fluctuations through the order-by-disorder mechanism. Indeed, simple analysis shows that these cubic directions allow for the largest number of zero modes at the harmonic level [55].

Importantly, although the spin-symmetry is seemingly reduced from spherical to cubic when crossing T_c, this cannot be viewed as a true reduction of symmetries as the Γ model itself is already cubic-symmetric. The apparent spherical symmetry at $T_c < T < |\Gamma|$ is an *emergent* property of the phase, which is due to spatial fluctuations of directional vector $\hat{\mathbf{n}}(\mathbf{r})$. Another important observation is that while the degeneracy associated with $\hat{\mathbf{n}}$ is lifted by thermal fluctuation, a discrete macroscopic degeneracy persists due to the Ising gauge symmetry of $\{\eta_\alpha\}$, especially for classical spins. Consequently, spins remain disordered at $T < T_c$.

To resolve this issue and investigate the nature of the low-T phase, we first note that the cubic spin-orbital symmetry of the Γ model is indeed broken below T_c, yet in a complicated pattern: local spins have to pick one of the six cubic directions in a coordinated way while preserving the gauge symmetry of $\{\eta_\alpha\}$. A convenient local quantity to characterize the broken symmetry is the flux variable defined on each hexagon [11]:

$$W_\alpha = S_1^x\, S_2^y\, S_3^z\, S_4^x\, S_5^y\, S_6^z, \tag{2}$$

where $\mathbf{S}_{1,\cdots,6}$ are the six spins around the α hexagon. These fluxes play an important role in the spin-1/2 Ki-

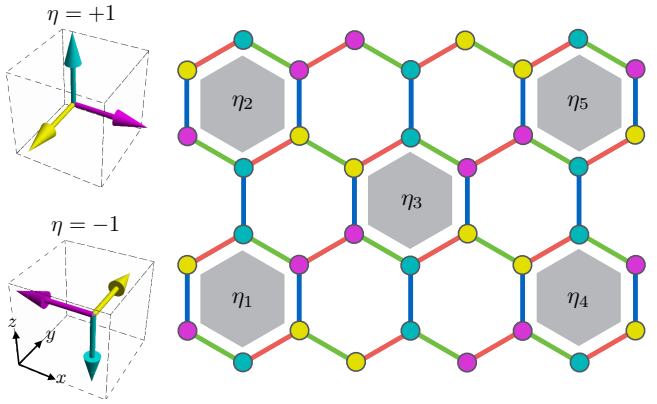

FIG. 3. (Color online) Plaquette order of hexagonal fluxes on honeycomb lattice. Shaded hexagons have nonzero flux $W \sim 1$, while empty hexagons have a vanishing W. Spins are orthogonal to each other (with left handedness for $\zeta = -1$) on each shaded hexagon; their specific directions depend on the local η, as specified in the insets. The arrangement of hexagons with finite W corresponds to the famous $\sqrt{3} \times \sqrt{3}$ long-range order. Spins remain disordered due to uncorrelated η_α on the shaded hexagons.

taev model as they are "integrals of motion" of the Hamiltonian [11]. In our case, the flux W_α is similarly a gauge-invariant variable, that is independent of η_α. On the other hand, it can be used to characterize the ordering of $\hat{\mathbf{n}}$. To see this, we note that in the ground state, they only take on three different values [50]: $W_\mathrm{A} = \zeta a^6$ for hexagons whose η is associated with component a, and similarly $W_\mathrm{B} = \zeta b^6$ and $W_\mathrm{C} = \zeta c^6$ for the other two sets of hexagons, where $\zeta = -\mathrm{sgn}(\Gamma)$. As $\hat{\mathbf{n}}$ freezes to one of the cubic directions, 2/3 of the fluxes also vanish. Since hexagons of a given type form an enlarged triangular lattice, the flux patten of the low-T phase, e.g. $W_A \approx 1$, and $W_B \approx W_C \approx 0$, corresponds to a broken translation symmetry; see Fig. 3. Importantly, the uncorrelated η_α on hexagons with nonzero W give rise to a disordered spin configuration. We note in passing that plaquette orders with similar spatial pattern also exist as ground state in J_1-J_2 quantum $S = 1/2$ and $S = 1$ honeycomb Heisenberg model [56–59]. Our finding shows a rare example of plaqutte ordering hidden in a classical spin liquid on honeycomb lattice.

The arrangement of hexagons with nonzero W shown in Fig. 3 suggests an order parameter

$$\tilde{W}(\mathbf{Q}) = \frac{1}{N} \sum_\alpha W_\alpha \, e^{i\mathbf{Q}\cdot\mathbf{r}_\alpha}, \qquad (3)$$

which is the Fourier transform at wavevector $\mathbf{Q} = (4\pi/3, 0)$, corresponding to the $\sqrt{3}\times\sqrt{3}$-order, for characterizing the broken translation symmetry. We performed extensive MC simulations at temperatures around T_c to examine the critical behaviors; the results are summarized in Fig. 4. The specific heat shows clear finite-size effect. Moreover, the order parameter defined as $\Phi \equiv \langle|\tilde{W}(\mathbf{Q})|\rangle$ exhibits characteristics of a second-order

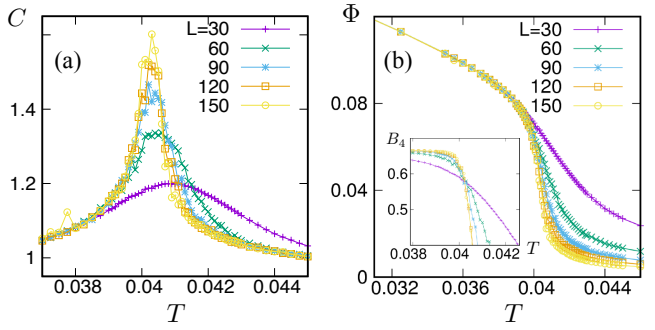

FIG. 4. (Color online) Monte Carlo simulation of the translation symmetry breaking of flux variables. (a) specific heat C, (b) order parameter $\Phi = \langle|\tilde{W}(\mathbf{Q})|\rangle$. The crossing point of the Binder curves (inset) gives an estimate of $T_c \approx 0.0402$ [60]. Critical exponents of the transition are obtained from finite-size scaling: $\alpha = 0.167$, $\beta = 0.177$, $\gamma = 1.47$, and $\nu = 0.863$.

phase transition. For example, the growth of Φ below T_c becomes sharper with increasing L. We estimate a critical temperature $T_c \approx 0.0402|\Gamma|$ from the crossing of B_4 curves [60]. Our finite-size scaling analysis produces fairly reasonable data-points collapsing [60], further supporting a second-order phase transition at T_c. Since the plaqute-ordering is intimately related to a broken Z_3 symmetry, some of the critical exponents, e.g. ν and γ, obtained from finite-size scaling, shown in caption of Fig. 4, are consistent with the 2D 3-state Potts universality class [61], although others show noticeable deviations. This discrepancy could be due to the gauge degrees of freedom $\{\eta_\alpha\}$, which might have nontrivial effects on the critical behavior.

We next investigate the dynamical behaviors of the spin liquids above and below the critical T_c. To this end, we employ the semiclassical Landau-Lifshitz (LL) dynamics simulation, which has been successfully applied to compute the dynamical structure factor of various classical spin liquids [9, 62, 63]. For $T > T_c$, MC simulations are used to prepare initial states sampled from the Boltzmann distribution. We then perform energy-conserving LL simulation to obtain trajectories of spins $\mathbf{S}_i(t)$ [64, 65]. The dynamical structure factor $\mathcal{S}^{\alpha\beta}(\mathbf{q},\omega)$ is computed from the Fourier transform of the real-space correlator $\langle S_i^\alpha(t) S_j^\beta(0)\rangle$, where $\alpha, \beta = x, y, z$, averaged over the initial states. As discussed above, since ground states parameterized by different $\{\eta_\alpha\}$ are disconnected below T_c, an additional average over random $\{\eta_\alpha\}$ is introduced manually to improve the efficiency [66, 67].

The diagonal part of the dynamical structure factor $\mathcal{S}(\mathbf{q},\omega) \equiv \sum_\alpha \mathcal{S}^{\alpha\alpha}(\mathbf{q},\omega)$ are shown in Fig. 5 for the two spin liquid phases. The $\mathcal{S}(\mathbf{q},\omega)$ at $T > T_c$ shows broad continuum over a wide energy range in both cases. On the other hand, structures of coherent quasi-particle dispersion can be seen at high energies for $\mathcal{S}(\mathbf{q},\omega)$ in the low-T phase. These coherent excitations in a liquid phase are reminiscent of the electron pseudo-bands observed in liquid metals [68, 69]. Their origin can be traced to the

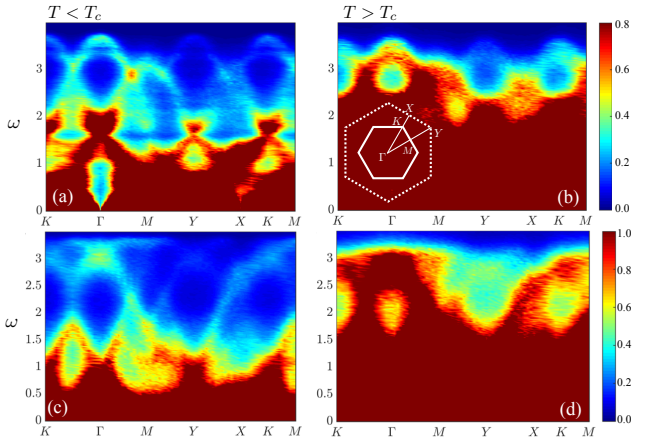

FIG. 5. (Color online) The diagonal part of the dynamical structure factor $\mathcal{S}(\mathbf{q},\omega) = \mathcal{S}^{xx}(\mathbf{q},\omega) + \mathcal{S}^{yy}(\mathbf{q},\omega) + \mathcal{S}^{zz}(\mathbf{q},\omega)$ computed from LL simulations for antiferromagnetic (top) and ferromagnetic (bottom) Γ model. The results below T_c are shown in panels (a) and (c), while those above T_c are shown in (b) and (d).

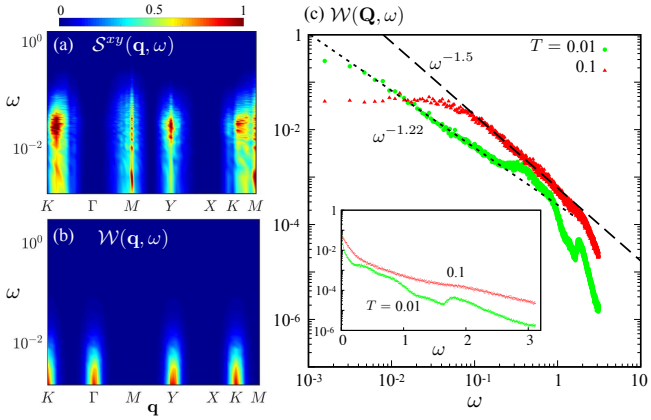

FIG. 6. (Color online) (a) Off-diagonal dynamical structure factor $\mathcal{S}^{xy}(\mathbf{q},\omega)$ in logarithmic scale, and (b) dynamical structure factor of flux variables $\mathcal{W}(\mathbf{q},\omega)$ in logarithmic scale at $T = 0.01$. Also note the log-scale for the ω axis. (c) The ω dependence of the flux dynamical structure factor $\mathcal{W}(\mathbf{Q},\omega)$ at the $\sqrt{3}\times\sqrt{3}$ ordering wavevector $\mathbf{Q}$ for both high and low-T spin liquid phases.

robust local or short-range ordering in a liquid state.

Interestingly, the off-diagonal $\mathcal{S}^{xy}(\mathbf{q},\omega)$, shown in Fig. 6(a), exhibits intriguing excitations associated with the high-symmetry points of the BZ. It is important to note that a large signal also exists at the same high-symmetry points in the *static* structure factor. These quasi-$\mathbf{q}$-independent features thus seem to derive from coherent oscillations of the underlying plaquette pattern. To further investigate the source of these excitations, we compute the dynamical structure factor of fluxes $\mathcal{W}(\mathbf{q},\omega)$, which is defined as the space-time Fourier transform of the correlation function $\langle W_\alpha(t)W_\beta(0)\rangle$. Interestingly, as shown in Fig. 6(b), similar momentum-specific excitations are observed in the dynamical structure factor $\mathcal{W}(\mathbf{q},\omega)$. In addition to the long-range order at the K-point, the finite excitations associated with the Γ and Y points result from the non-zero average $\langle W\rangle \approx 1/3$ of the $\sqrt{3}\times\sqrt{3}$ flux patterns, e.g. $W_A \approx 1$, and $W_B \approx W_C \approx 0$.

Fig. 6(c) and its inset show the ω dependence of the dynamical excitations $\mathcal{W}(\mathbf{Q},\omega)$ with momentum fixed at $\mathbf{Q} = (4\pi/3, 0)$, corresponding to the K point. Significant differences in the overall behavior can be seen at temperatures above and below the critical T_c, in particular see the inset semi-log plot. Importantly, we find distinct power-law behaviors $\mathcal{W}(\mathbf{Q},\omega) \sim 1/\omega^a$ in the two spin-liquid phases, with the exponent $a \approx 1.5$ at high temperatures, and $a \approx 1.22$ in the flux-ordered phase. These exponents might be related to the critical behavior of the disorder-induced localization of the low-energy spin-excitations [70, 71]. These finite energy excitations at the ordering wavevector $\mathbf{Q}$ reflect the composite nature of the flux variables that develop a long range order below T_c. Notably, they are in stark contrast to the dispersive Goldstone modes of simple long-range magnetically ordered states.

Discussion and Outlook. We have demonstrated that thermal order-by-disorder in honeycomb Γ-model drives a phase transition into a new spin liquid phase with a hidden flux long-range order. In the presence of other perturbations, the degeneracy of the plaquette-ordered states is lifted. Specifically, the antiferro-Kitaev exchange preserves the continuous degeneracy of $\hat{\mathbf{n}} = (a, b, c)$, while lifting the discrete η degeneracy by selecting the uniform configuration. Interestingly. the discrete degeneracy remains in the case of ferromagnetic Kitaev exchange. On the other hand, Heisenberg interactions favors a ground state with $\hat{\mathbf{n}} = (1, 1, 1)$. However, the flux-ordered spin liquid is expected to survive in a finite temperature window when these perturbations are small compared with the dominant Γ term. In the presence of a magnetic field along the [111] direction, the flux-ordered liquid phase also survives up to $H_c \sim 0.3|\Gamma|$, above which a distinct intermediate phase sets in as the ground state. Experimentally, through coupling to other degrees of freedom in crystal, e.g. spin-lattice coupling, the translation-symmetry breaking could produce Bragg peaks in neutron or X-ray scattering.

The effects of quantum fluctuations have been extensively discussed in Ref. [50]. The relevant energy scale of quantum order-by-disorder is $T^* \sim \mathcal{O}(|\Gamma|S)$ for both the discrete η and continuous $\hat{\mathbf{n}}$ variables [50]. As noted in the same study, the induced effective interaction between η_α remains frustrated for antiferromagnetic Γ, so a similar flux-ordered spin liquid can be stabilized by pure quantum fluctuations in this case. It is, however, unclear what is the scenario in the ferromagnetic Γ model due to the closeness of the two energy scales. Restoring the spin length, the critical temperature for thermal order-by-disorder is $T_c \sim 0.04|\Gamma|S^2$. Our finding thus ensures the existence of the exotic flux-ordered spin liquid for

large S at the temperature window $T^* \lesssim T \lesssim T_c$. Finally, it is also of great interest to study similar flux-ordering in three-dimensional hyper- or stripy-honeycomb lattices where some of the flux variables are defined on extended strings.

Acknowledgements. The authors thank C. D. Batista, N. Perkins, and I. Rousochatzakis for useful discussions. G.-W. C. acknowledges support from the Center for Materials Theory as a part of the Computational Materials Science (CMS) program, funded by the DOE Office of Science, Basic Energy Sciences, Materials Sciences and Engineering Division.

Note added: Upon finishing our manuscript, we became aware that dynamical structure factor of the Γ-model has also been studied in [72].

[1] W. Witczak-Krempa, G. Chen, Y. B. Kim, and L. Balents, Correlated Quantum Phenomena in the Strong Spin-Orbit Regime, Annu. Rev. Condens. Matter Phys. **5**, 57 (2014).
[2] K. Kugel and D. I. Khomskii, The Jahn-Teller effect and magnetism: transition metal compounds, Sov. Phys. Usp. **25**, 231 (1982).
[3] Z. Nussinov and J. van den Brink, Compass models: Theory and physical motivations, Rev. Mod. Phys. **87**, 1 (2015).
[4] C. Wu, Orbital Ordering and Frustration of p-Band Mott Insulators, Phys. Rev. Lett. **100**, 200406 (2008).
[5] E. Zhao and W. V. Liu, Orbital Order in Mott Insulators of Spinless p-Band Fermions, Phys. Rev. Lett. **100**, 160403 (2008).
[6] G.-W. Chern and C. Wu, Orbital ice: An exact Coulomb phase on the diamond lattice, Phys. Rev. E **84**, 061127 (2011).
[7] J. T. Chalker, P. C. W. Holdsworth, and E. F. Shender, Hidden order in a frustrated system: Properties of the Heisenberg Kagome antiferromagnet, Phys. Rev. Lett. **68**, 855 (1992).
[8] G.-W. Chern and R. Moessner, Dipolar Order by Disorder in the Classical Heisenberg Antiferromagnet on the Kagome Lattice, Phys. Rev. Lett. **110**, 077201 (2013).
[9] R. Moessner and J. T. Chalker, Properties of a Classical Spin Liquid: The Heisenberg Pyrochlore Antiferromagnet, Phys. Rev. Lett. **80**, 2929 (1998)
[10] see, e.g. C. Lacroix, P. Mendels, and F. Mila, *Introduction to Frustrated Magnetism: Materials, Experiments, Theory*, Springer Series in Solid-State Sciences (Springer, Berlin, 2011).
[11] A. Kitaev, Anyons in an exactly solved model and beyond, Ann. Phys. (Amsterdam) **321**, 2 (2006).
[12] J. Knolle, D. L. Kovrizhin, J. T. Chalker, and R. Moessner, Dynamics of a Two-Dimensional Quantum Spin Liquid: Signatures of Emergent Majorana Fermions and Fluxes, Phys. Rev. Lett. **112**, 207203 (2014).
[13] J. Nasu, M. Udagawa, and Y. Motome, Vaporization of Kitaev Spin Liquids, Phys. Rev. Lett. **113**, 197205 (2014).
[14] G. Baskaran, D. Sen, and R. Shankar, Spin-S Kitaev model: Classical ground states, order from disorder, and exact correlation functions, Phys. Rev. B **78**, 115116 (2008).
[15] S. Chandra, K. Ramola, and D. Dhar, Classical Heisenberg spins on a hexagonal lattice with Kitaev couplings, Phys. Rev. E **82**, 031113 (2010).
[16] C. C. Price and N. B. Perkins, Critical Properties of the Kitaev-Heisenberg Model, Phys. Rev. Lett. **109**, 187201 (2012).
[17] I. Rousochatzakis, Y. Sizyuk, and N. B. Perkins, Quantum spin liquid in the semiclassical regime, Nat. Commun. **9**, 1575 (2018).
[18] G. Jackeli and G. Khaliullin, Mott Insulators in the Strong Spin-Orbit Coupling Limit: From Heisenberg to a Quantum Compass and Kitaev Models, Phys. Rev. Lett. **102**, 017205 (2009).
[19] J. Chaloupka, G. Jackeli, and G. Khaliullin, Kitaev-Heisenberg Model on a Honeycomb Lattice: Possible Exotic Phases in Iridium Oxides A_2IrO_3, Phys. Rev. Lett. **105**, 027204 (2010).
[20] J. Chaloupka, G. Jackeli, and G. Khaliullin, Zigzag Magnetic Order in the Iridium Oxide Na_2IrO_3, Phys. Rev. Lett. **110**, 097204 (2013).
[21] S. Trebst, Kitaev Materials, arXiv:1701.07056 (2017).
[22] Y. Singh, S. Manni, J. Reuther, T. Berlijn, R. Thomale, W. Ku, S. Trebst, and P. Gegenwart, Relevance of the Heisenberg-Kitaev Model for the Honeycomb Lattice Iridates A_2IrO_3, Phys. Rev. Lett. **108**, 127203 (2012).
[23] F. Ye, S. Chi, H. Cao, B. C. Chakoumakos, J. A. Fernandez-Baca, R. Custelcean, T. F. Qi, O. B. Korneta, and G. Cao, Direct evidence of a zigzag spin-chain structure in the honeycomb lattice: A neutron and x-ray diffraction investigation of single-crystal Na_2IrO_3, Phys. Rev. B **85**, 180403(R) (2012).
[24] S. K. Choi, R. Coldea, A. N. Kolmogorov, T. Lancaster, I. I. Mazin, S. J. Blundell, P. G. Radaelli, Yogesh Singh, P. Gegenwart, K. R. Choi, S.-W. Cheong, P. J. Baker, C. Stock, and J. Taylor, Spin Waves and Revised Crystal Structure of Honeycomb Iridate Na_2IrO_3, Phys. Rev. Lett. 108, 127204 (2012).
[25] S. Hwan Chun, J.-W. Kim, J. Kim, H. Zheng, C. C. Stoumpos, C. D. Malliakas, J. F. Mitchell, K. Mehlawat, Y. Singh, Y. Choi, T. Gog, A. Al-Zein, M. M. Sala, M. Krisch, J. Chaloupka, G. Jackeli, G. Khaliullin, and B. J. Kim, Direct evidence for dominant bond-directional interactions in a honeycomb lattice iridate Na_2IrO_3, Nat. Phys. **11**, 462 (2015).
[26] S. C. Williams, R. D. Johnson, F. Freund, S. Choi, A. Jesche, I. Kimchi, S. Manni, A. Bombardi, P. Manuel, P. Gegenwart, and R. Coldea, Incommensurate counterrotating magnetic order stabilized by Kitaev interactions in the layered honeycomb α-Li_2IrO_3, Phys. Rev. B **93**, 195158 (2016).
[27] K. W. Plumb, J. P. Clancy, L. J. Sandilands, V. V. Shankar, Y. F. Hu, K. S. Burch, H.-Y. Kee, and Y.-J. Kim, α-$RuCl_3$: A spin-orbit assisted Mott insulator on a honeycomb lattice, Phys. Rev. B **90**, 041112 (2014).
[28] J. A. Sears, M. Songvilay, K. W. Plumb, J. P. Clancy, Y. Qiu, Y. Zhao, D. Parshall, and Y.-J. Kim, Magnetic order in α-$RuCl_3$: A honeycomb-lattice quantum magnet with strong spin-orbit coupling, Phys. Rev. B **91**, 144420 (2015).
[29] Y. Kubota, H. Tanaka, T. Ono, Y. Narumi, and K. Kindo, Successive magnetic phase transitions in α-$RuCl_3$:

XY-like frustrated magnet on the honeycomb lattice, Phys. Rev. B **91**, 094422 (2015).
[30] R. D. Johnson, S. C. Williams, A. A. Haghighirad, J. Singleton, V. Zapf, P. Manuel, I. I. Mazin, Y. Li, H. O. Jeschke, R. Valenti, and R. Coldea, Monoclinic crystal structure of α-$RuCl_3$ and the zigzag antiferromagnetic ground state, Phys. Rev. B **92**, 235119 (2015).
[31] A. Biffin, R. D. Johnson, S. Choi, F. Freund, S. Manni, A. Bombardi, P. Manuel, P. Gegenwart, and R. Coldea, Unconventional magnetic order on the hyperhoneycomb Kitaev lattice in β-Li_2IrO_3: Full solution via magnetic resonant x-ray diffraction, Phys. Rev. B **90**, 205116 (2014).
[32] A. Biffin, R. D. Johnson, I. Kimchi, R. Morris, A. Bombardi, J. G. Analytis, A. Vishwanath, and R. Coldea, Noncoplanar and Counterrotating Incommensurate Magnetic Order Stabilized by Kitaev Interactions in γ-Li_2IrO_3, Phys. Rev. Lett. **113**, 197201 (2014).
[33] K. Modic, T. E. Smidt, I. Kimchi, N. P. Breznay, A. Biffin, S. Choi, R. D. Johnson, R. Coldea, P. Watkins-Curry, and G. T. McCandess et al., Realization of a three-dimensional spin anisotropic harmonic honeycomb iridate, Nat. Commun. **5**, 4203 (2014).
[34] J. Zheng, K. Ran, T. Li, J. Wang, P. Wang, B. Liu, Z.-X. Liu, B. Normand, J. Wen, and W. Yu, Gapless Spin Excitations in the Field-Induced Quantum Spin Liquid Phase of α-$RuCl_3$, Phys. Rev. Lett. **119**, 227208 (2017).
[35] Z. Wang, S. Reschke, D. Hüvonen, S.-H. Do, K.-Y. Choi, M. Gensch, U. Nagel, T. Room, and A. Loidl, Magnetic Excitations and Continuum of a Possibly Field-Induced Quantum Spin Liquid in α-$RuCl_3$, Phys. Rev. Lett. **119**, 227202 (2017).
[36] S.-H. Baek, S.-H. Do, K.-Y. Choi, Y. S. Kwon, A. U. B. Wolter, S. Nishimoto, Jeroen van den Brink, and B. Büchner, Evidence for a Field-Induced Quantum Spin Liquid in α-$RuCl_3$, Phys. Rev. Lett. **119**, 037201 (2017).
[37] T. Takayama, A. Kato, R. Dinnebier, J. Nuss, H. Kono, L. S. I. Veiga, G. Fabbris, D. Haskel, and H. Takagi, Hyperhoneycomb Iridate β-Li_2IrO_3 as a Platform for Kitaev Magnetism, Phys. Rev. Lett. **114**, 077202 (2015).
[38] L. S. I. Veiga, M. Etter, K. Glazyrin, F. Sun, C. A. Escanhoela, Jr., G. Fabbris, J. R. L. Mardegan, P. S. Malavi, Y. Deng, P. P. Stavropoulos, H.-Y. Kee, W. G. Yang, M. van Veenendaal, J. S. Schilling, T. Takayama, H. Takagi, and D. Haskel, Pressure tuning of bond- directional exchange interactions and magnetic frustration in the hyperhoneycomb iridate β-Li_2IrO_3, Phys. Rev. B 96, 140402(R) (2017).
[39] Y. Sizyuk, C. Price, P. Wölfle, and N. B. Perkins, Importance of anisotropic exchange interactions in honeycomb iridates: Minimal model for zigzag antiferromagnetic order in Na_2IrO_3, Phys. Rev. B **90**, 155126 (2014).
[40] J. G. Rau, E. K.-H. Lee, and H.-Y. Kee, Generic Spin Model for the Honeycomb Iridates beyond the Kitaev Limit, Phys. Rev. Lett. **112**, 077204 (2014).
[41] S. M. Winter, Y. Li, H. O. Jeschke, and R. Valenti, Challenges in design of Kitaev materials: Magnetic interactions from competing energy scales, Phys. Rev. B **93**, 214431 (2016).
[42] H.-S. Kim and H.-Y. Kee, Crystal structure and magnetism in α-$RuCl_3$: An ab initio study, Phys. Rev. B **93**, 155143 (2016).
[43] J. Chaloupka and G. Khaliullin, Magnetic anisotropy in the Kitaev model systems Na_2IrO_3 and $RuCl_3$, Phys. Rev. B **94**, 064435 (2016).
[44] S. Nishimoto, V. M. Katukuri, V. Yushankhai, H. Stoll, U. K. Roessler, L. Hozoi, I. Rousochatzakis, and J. van den Brink, Strongly frustrated triangular spin lattice emerging from triplet dimer formation in honeycomb Li_2IrO_3, Nat. Commun. **7**, 10273 (2016).
[45] L. Janssen, E. C. Andrade, and M. Vojta, Magnetization processes of zigzag states on the honeycomb lattice: Identifying spin models for α-$RuCl_3$ and Na_2IrO_3, Phys. Rev. B **96**, 064430 (2017).
[46] S. M. Winter, K. Riedl, R. A. Maksimov, A. L. Chernyshev, A. Honecker, and R. Valenti, Breakdown of magnons in a strongly spin-orbital coupled magnet, Nat. Commun. **8**, 1152 (2017).
[47] Z.-X. Liu and B. Normand, Dirac and chiral quantum spin liquids on the honeycomb lattice in a magnetic field, Phys. Rev. Lett. **120**, 187201 (2018).
[48] H.-S. Kim, Y. B. Kim, and H.-Y. Kee, Revealing frustrated local moment model for pressurized hyperhoneycomb iridate: Paving the way toward a quantum spin liquid, Phys. Rev. B **94**, 245127 (2016).
[49] M. Majumder, R. S. Manna, G. Simutis, J. C. Orain, T. Dey, F. Freund, A. Jesche, R. Khasanov, P. K. Biswas, E. Bykova, N. Dubrovinskaia, L. S. Dubrovinsky, R. Yadav, L. Hozoi, S. Nishimoto, A. A. Tsirlin, and P. Gegenwart, Breakdown of magnetic order in the pressurized Kitaev iridate, Phys. Rev. Lett. **120**, 237202 (2018).
[50] I. Rousochatzakis and N. B. Perkins, Classical spin liquid instability driven by off-diagonal exchange in strong spin-orbital magnets, Phys. Rev. Lett. **118**, 147204 (2017).
[51] See supplemental materials for details of Monte Carlo simulations and the calculation of static structure factors.
[52] D. A. Garanin and B. Canals, Classical spin liquid: Exact solution for the infinite-component antiferromagnetic model on the kagome lattice, Phys. Rev. B **59**, 443 (1999).
[53] S. V. Isakov, K. Gregor, R. Moessner, and S. L. Sondhi, Dipolar Spin Correlations in Classical Pyrochlore Magnets, Phys. Rev. Lett. **93**, 167204 (2004).
[54] C. L. Henley, Power-law spin correlations in pyrochlore antiferromagnets, Phys. Rev. B **71**, 014424 (2005).
[55] See supplemental materials for details on the calculation of zero modes. Related techniques can be found in Ref. [9] (first reference in the supplementary material).
[56] R. Ganesh, J. van den Brink, and S. Nishimoto, Deconfined Criticality in the Frustrated Heisenberg Honeycomb Antiferromagnet, Phys. Rev. Lett. **110**, 127203 (2013).
[57] Z. Zhu, D. A. Huse, and S. R. White, Weak Plaquette Valence Bond Order in the $S = 1/2$ Honeycomb J_1-J_2 Heisenberg Model, Phys. Rev. Lett. **110**, 127205 (2013).
[58] H. H. Zhao, Cenke Xu, Q. N. Chen, Z. C. Wei, M. P. Qin, G. M. Zhang, and T. Xiang, Plaquette order and deconfined quantum critical point in the spin-1 bilinear-biquadratic Heisenberg model on the honeycomb lattice, Phys. Rev. B **85**, 134416 (2012).
[59] S.-S. Gong, W. Zhu, and D. N. Sheng, Quantum phase diagram of the spin-1 J_1-J_2 Heisenberg model on the honeycomb lattice, Phys. Rev. B **92**, 195110 (2015).
[60] See supplemental materials for details of Monte Carlo simulations and finite-size scaling analysis of the thermal order-by-disorder transition.
[61] F. Y. Wu, The Potts model, Rev. Mod. Phys. **54**, 235 (1982).
[62] M. Taillefumier, J. Robert, C. L. Henley, R. Moessner, and B. Canals, Semiclassical spin dynamics of the anti-

ferromagnetic Heisenberg model on the kagome lattice, Phys. Rev. B **90**, 064419 (2014).
[63] A. M. Samarakoon, A. Banerjee, S.-S. Zhang, Y. Kamiya, S. E. Nagler, D. A. Tennant, S.-H. Lee, and C. D. Batista, Comprehensive study of the dynamics of a classical Kitaev spin liquid, Phys. Rev. B **96**, 134408 (2017).
[64] J. H. Mentink, M. V. Tretyakov, A. Fasolino, M. I. Katsnelson, and Th. Rasing, Stable and fast semi-implicit integration of the stochastic Landau-Lifshitz equation, J. Phys.: Cond. Matter **22**, 176001 (2010).
[65] Details of the Landau-Lifshitz dynamics simulation can be found in the Supplementary materials.
[66] Since the effective interaction between the Ising variables $\{\eta_\alpha\}$ is frustrated, special Monte Carlo sampling of the antiferromagnetic Ising model on the triangle lattice [67] was performed for the initial state; see supplemental material for details.
[67] G. H. Wannier, Antiferromagnetism. The Triangular Ising Net, Phys. Rev. **79**, 357 (1950).
[68] F. Baumberger, W. Auwärter, T. Greber, J. Osterwalder, Electron Coherence in a Melting Lead Monolayer, Science **306**, 2221 (2004).
[69] K. S. Kim and H. W. Yeom, Radial Band Structure of Electrons in Liquid Metals, Phys. Rev. Lett. **107**, 136402 (2011).
[70] Power-law ω-dependence of $\mathcal{S}(\mathbf{q},\omega)$ in the vicinity of Bragg peaks has been investigated in, e.g. Ref. [71]. Detailed study of these low-energy spin-excitations will be left in the future.
[71] R. Bruinsma and S. N. Coppersmith, Anderson localization and breakdown of hydrodynamics in random ferromagnets, Phys. Rev. B **33**, 6541 (1986).
[72] A. M. Samarakoon, G. Wachtel, Y. Yamaji, D. A. Tennant, C. D. Batista, Y. B. Kim, Classical and quantum spin dynamics of the honeycomb Γ model, Phys. Rev. B **98**, 045121 (2018).